16

Biological Applications of FM-AFM in Liquid Environment

Takeshi Fukuma and Suzanne P. Jarvis

Abstract. Atomic force microscopy (AFM) was noted for its potential to study biological materials shortly after its first development in 1986 due to its ability to image insulators in liquid environments. The subsequent application of AFM to biology has included lateral characterization via imaging, unraveling of molecules under a tensile load and application of a force either to measure mechanical properties under the tip or to instigate a biochemical response in living cells. To date, the application of frequency modulation AFM (FM-AFM) specifically to biological materials has been limited to relatively few research groups when compared to the extensive application of AFM to biological materials. This is probably due to the perceived complexity of the technique both by researchers in the life sciences and those manufacturing liquid AFMs for biological research. In this chapter, we aim to highlight the advantages of applying the technique to biological materials.

16.1 Quantitative Force Measurements

One of the advantages of the FM-AFM technique in any environment is that when operated in constant-amplitude mode it implicitly decouples the influence of conservative and dissipative forces. To fully take advantage of this fact it is necessary to be able to both implement the technique correctly and convert the resulting frequency shifts and driving signals into quantitative measures of conservative and dissipative interaction forces. In this section we discuss the quantification of FM-AFM and issues arising from the method of implementation.

16.1.1 Calculating Force from Frequency Shift

In contrast to the simple Hooke's law relation connecting the static deflection of a cantilever to the interaction force, the corresponding relation for FM-AFM is significantly more complex and depends on both the spring constant and amplitude of oscillation of the cantilever. This relation was first derived by Giessibl [1], and is valid for any amplitude of oscillation:

S. Morita et al. (eds.), *Noncontact Atomic Force Microscopy*,
NanoScience and Technology,
DOI: 10.1007/978-3-642-01495-6_16,

$$\frac{\Delta\omega}{\omega_0} = -\frac{1}{\pi Ak}\int_{-1}^{1} F(z + A(1+u))\frac{u}{\sqrt{1-u^2}}\mathrm{d}u, \tag{16.1}$$

where k is the spring constant of the cantilever, F the interaction force between tip and sample, ω_0 its unperturbed resonant frequency, $\Delta\omega$ the change in resonant frequency, A the amplitude of oscillation, and z is the distance of closest approach between tip and sample.

To determine the interaction force from the observed frequency shift, (16.1) must be inverted. For many years this has been performed analytically for cases where the amplitude of oscillation was far smaller or greater than all characteristic length scales of the interaction force [2,3]. However, use of these limiting formulas in practice can potentially lead to significant errors, unless the precise nature of the force is known. This is particularly problematic if the interaction force contains a spectrum of length scales, encompassing short- to long-range components, as is often the case. In such situations, it is possible that the oscillation amplitude may be considered small with respect to long-range components, but large for short-range components. Accurate determination of the interaction force may therefore not be possible using these limiting formulas.

A simple yet accurate analytical formula that enables the direct determination of the interaction force from the measured frequency shift was proposed by Sader and Jarvis in 2004:

$$F(z) = 2k\int_{z}^{\infty}\left(1 + \frac{A^{1/2}}{8\sqrt{\pi(1-z)}}\right)\Omega(t) - \frac{A^{3/2}}{\sqrt{2(t-z)}}\frac{\mathrm{d}\Omega(t)}{\mathrm{d}t}\mathrm{d}t, \tag{16.2}$$

where $\Omega(z) = \Delta\omega(z)/\omega_0$. This formula has been shown to be both mathematically and experimentally robust [4,5], is valid for any amplitude of oscillation and is applicable to any force law. However, it is only valid when the amplitude of oscillation is kept constant (i.e., it is not applicable to constant excitation FM-AFM). Further, an inherent assumption in deriving this formula is that the interaction force is continuous. This is not the case when discontinuities occur due to bond breaking as is the case in single molecule spectroscopy measurements. Thus, care must be taken in these experiments to only apply the formula in the region where this assumption is valid. It should also be noted that this formula assumes that the resonance condition is met. If the measurements are made off resonance (this can easily be done in error in low Q environments such as liquid) then the correct force is only retrieved if the phase error is known and accounted for in the calculation [6,7].

16.1.2 Cantilever Excitation in Liquid

For operation, FM-AFM requires mechanical excitation of the cantilever at the resonance frequency. When investigating biological samples either piezo activation or magnetic activation [8] has been chosen. The piezo activation

method is usually considered the easiest activation method to implement because it does not require any modification to standard commercial cantilevers. In this case, a small piece of piezoelectric actuator is placed adjacent to the cantilever holder. An alternating voltage signal, which is referred to as the cantilever excitation signal, is applied across the actuator to induce a vibration. This vibration is transmitted through the cantilever holder and cantilever base to the cantilever itself. Since the actuator does not directly drive the cantilever end but instead drives it via other mechanical elements, the vibration of the actuator excites the resonances of all the elements mechanically coupled with the actuator. Consequently, the phase and amplitude of the deflection signal can be influenced by the spurious resonances that do not represent the true cantilever vibration characteristics. Such influence can lead to an error in the quantification of force from frequency shift and dissipation measurements. It can also prevent stable cantilever vibration especially in FM-AFM, where the phase information of the deflection signal is used in the self-excitation circuit. Such influence is often a serious problem in liquid. The Q-factor in liquid (typically $Q < 10$) is much lower than that in air and vacuum so that the phase delay and amplitude distortion induced by the spurious resonances are not negligible. In addition, the actuator is mechanically coupled with additional elements (e.g., the liquid cell) through the liquid. This forms a complicated mechanical transmission path through which the vibration energy of the actuator can excite a number of spurious resonances.

To avoid any influence from spurious resonances, it is desirable to apply an excitation force directly to the end of the cantilever. Magnetic activation [8] fulfills this requirement. With this method, the cantilever is usually modified to have magnetic sensitivity either by coating it with a thin magnetic film or attaching a magnetic particle on the backside of the cantilever. The film, or the particle, is magnetized by applying a strong magnetic field. With this configuration an excitation signal is fed into a $V - I$ converter, which drives a coil placed close to the cantilever (usually underneath the sample), to produce an alternating magnetic field at the frequency of the cantilever resonance. The coil is usually aligned such that the interaction between the alternating magnetic field and the magnetic moment of the modified cantilever gives rise to a magnetic force perpendicular to the cantilever in order to excite the cantilever vibration normal to the surface. In an alternative arrangement of magnetic activation, cantilever actuation is achieved by passing an alternating electric current through a triangular cantilever. Thus, forming a current loop with a magnetic moment perpendicular to the plane of the cantilever. When placed at an angle in a static magnetic field, a force proportional to the current through the cantilever is generated [9].

The difference in measured amplitude and phase vs. frequency response obtained for the two different activation techniques with the same cantilever can be seen in Fig. 16.1a for piezo activation and Fig. 16.1b for magnetic excitation. The curves obtained with magnetic excitation show the typical amplitude and phase response of a simple harmonic oscillator while those

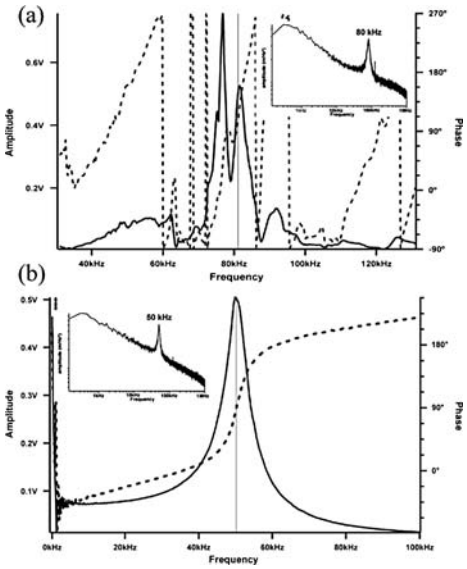

Fig. 16.1. Amplitude and phase vs. frequency characteristics of (**a**) cantilever oscillated in a liquid with a piezo excitation and (**b**) magnetic excitation. The insets show fast fourier transform spectra of the cantilever deflection signals showing thermal brownian vibration peaks (Reused with permission from Higgins et al. [10]. Copyright 2005, Institute of Physics)

obtained with piezo excitation show a number of spurious peaks. Simple phase vs. frequency characteristic are desirable for stable operation and quantitative measurements by FM-AFM, where the phase information is used for driving the cantilever.

16.1.3 Single Molecule Spectroscopy

FM-AFM being a relatively new technique, many applications of FM-AFM to biology have involved model samples that have already been studied extensively by other AFM techniques. In such cases, the primary motivation has been to characterize the FM technique itself rather than to elucidate new information about the chosen sample. In some cases new information has been obtained by utilizing the unique capability of FM-AFM to separate out conservative and dissipative components of the interaction, while in other cases it has been the enhanced sensitivity of the technique in comparison to alternative dynamic techniques which has revealed previously unobservable phenomena.

The first application of FM-AFM (actually FM-AFM combined with Q control) to a biological sample utilized the capacity of FM-AFM to separate out conservative and dissipative components of the interaction to estimate

the effective viscosity of a single dextran molecule [11]. In this measurement, FM-AFM was not applied in imaging mode but instead the technique was applied to single molecule force spectroscopy and found to provide significant improvement over conventional dynamic and static measurements. Specifically, they were able to measure a phase transition during the elongation of the dextran molecule and its effective viscosity to be 6,000 Pa·s, information not accessible with conventional static force spectroscopy. Although this experiment used oscillation amplitudes of approximately 10 nm this was still at least 1 order-of-magnitude smaller than the length of the dextran molecules and as such the magnitude of the oscillation was not found to be detrimental to the measurement. Similar measurements of dextran were subsequently made by the same group using transverse oscillations of a vertically mounted probe, the stiffness of which negated the addition of active Q control to achieve the same results [12].

The impact of oscillation amplitude in FM-AFM single molecule force spectroscopy was investigated in more detail with the mechanical unfolding of tandem repeats of titin I27 domains [13]. Unfolding intermediates were observed in each unfolded domain, which had not been observed previously with conventional force spectroscopy. The sensitivity of the FM technique to these intermediates was found to be related to the oscillation amplitude of the cantilever with smaller oscillation amplitudes providing higher sensitivity, as expected. In these measurements the smallest stable oscillation amplitude was 4.5 nm.

FM-AFM has also been applied to the measurement of ligand-receptor interactions, where the well-studied biotin–avidin system was chosen [10]. In this case, the mean unbinding force of a single unbinding event was found to be significantly higher than any measurements made with static force microscopy at different retraction rates. This was attributed to the significantly higher velocities achieved with FM-AFM, where the tip velocity is dependent on the resonant frequency and the oscillation amplitude of the cantilever (in this case 16.8 kHz and 6.3 nm, respectively). In the case of static-mode AFM, tip velocities are governed by z-piezo velocity and are typically limited to around 103 nm/s or less due to hydrodynamic drag forces.

16.2 Subnanometer-Resolution Imaging

16.2.1 Overview

Many examples of FM-AFM imaging of biological materials performed in the early stage have focused on comparing variations in experimental technique either by comparing the FM-AFM technique to other dynamic methods, comparing different feedback parameters within the FM-AFM technique or variations of the FM-AFM technique such as constant excitation FM-AFM

or FM-AFM plus Q control. Most of these comparisons were made with relatively large oscillation of the cantilever typically around 10 nm in amplitude which as we will see in Sect. 16.2.2 would have substantially decreased the overall sensitivity of the technique.

The first application of FM-AFM to imaging a biological sample was performed in 2001 by Tamayo et al. FM-AFM was again combined with Q control. In this case, living rat kidney cells were imaged with cantilever oscillation amplitudes typically in the region of 10 nm and imaging forces of less than 100 pN. Although the image was obtained as a frequency shift variation, the tip–sample distance regulation was made by keeping the oscillation amplitude constant. Thus, one may call it amplitude-modulation AFM rather than FM-AFM, depending on the definition. Although scan sizes were of the order of microns and the limits to resolution were consequently not explored, the authors note higher resolution than with the conventional tapping mode technique (see Fig. 11 in [14]) and predict that the technique may one day have comparable sensitivity to the optical tweezers technique. The authors highlight that at this level of sensitivity new interactions must be considered, in particular the role of confined liquid between tip and sample (Fig. 16.2) [15].

The low level of applied force during FM-AFM imaging was also observed by Sekiguchi et al. who used fragile protein aggregates known as amyloid fibrils in phosphate buffered saline to compare frequency feedback with amplitude feedback for a self-oscillating cantilever with a fixed driving amplitude

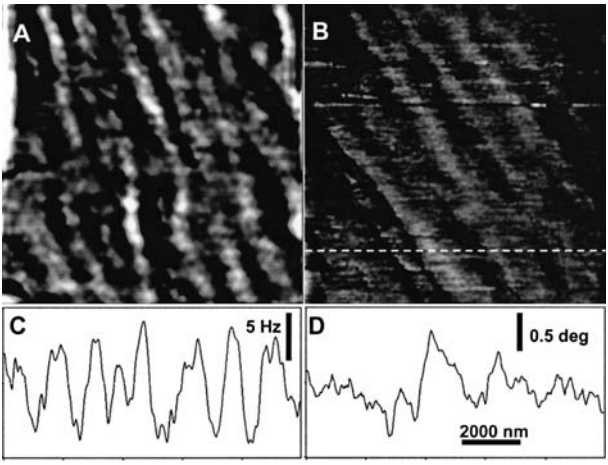

Fig. 16.2. (**a**) Resonant frequency image of a living rat kidney cell produced by combining FM-AFM and Q control. (**b**) Phase shift image of the same region with conventional tapping mode AFM in liquid. (**c**) and (**d**) are the profiles along the same scan line in (**a**) and (**b**). The scan line is marked in (**b**) with a *dashed line*. Scan size is $10 \times 10\,\mu$m. (Reused with permission from Tamayo et al. [14] Copyright 2001, Biophysical Society)

(constant excitation FM-AFM) [16]. They found a positive shift of the frequency to be more sensitive than a decrease in the amplitude (free lever amplitude 10 nm) and therefore used the frequency signal as the feedback signal for nondestructive imaging of the amyloid fibrils . They found that nondestructive imaging could only be achieved with an imaging force of 100 pN or less for these soft protein aggregates.

A similar comparison, this time between amplitude modulation AFM (AM-AFM) and FM-AFM imaging of DNA was made in pure water [17]. The cantilever amplitude during imaging was the same in both cases (4.8 nm), although the distance over which a frequency shift could be detected prior to hard contact with the sample, was approximately four times longer in the case of FM-AFM than the distance over which a decrease in cantilever amplitude could be detected in the case of AM-AFM. Thus the intermittent force applied could be more accurately controlled resulting in higher resolution and less sample deformation using FM-AFM.

Ebling et al. combined Q control with constant-excitation FM-AFM and directly compared the effect of enhanced Q when imaging DNA and a DPPC lipid bilayer lipid bilayers deposited onto a mica surface [18]. Feedback operated on change in amplitude of the cantilever and was set as close as possible to the free lever amplitude (typically 7 nm or greater) while still maintaining a stable image. In both cases increased corrugation of the topography was observed and attributed to a reduction of tip–sample indentation force.

While most comparisons have been made between different implementations of various dynamic techniques, in 2006 Hoogenboom et al. [19] made a direct comparison of constant-force contact mode images with FM-AFM images of bacteriorhodopsin formed with oscillation amplitudes in the range 0.64–1.00 nm. In their case, they note that higher normal forces were actually applied using the FM-AFM technique ($\sim$300 pN) although lateral forces were clearly minimized. In this case, the resolution appeared to be worse than that obtained using constant-force contact mode. Again using oscillation amplitudes of $\sim$1 nm but lower applied forces of $<$100 pN Hoogenboom et al. subsequently used FM-AFM to image various oligomeric states of voltage-dependent anion channels [20]. Although, in this case, FM-AFM allowed them to image with higher resolution they attributed this to a lack of lateral forces and still noted height inaccuracies in their FM-AFM images that they attributed to larger indentation forces than those observed in contact mode.

In 2006, Higgins et al. combined both imaging and force spectroscopy FM-AFM to investigate hydration at the membrane-fluid interfaces of two different supported lipid bilayers as a function of bilayer fluidity [21]. In this case the FM technique was utilized for its sensitivity and stability especially in regions of high attractive force gradients which result from the oscillatory nature of the force profile caused by the removal of successive hydration layers in the near surface region. The technique was found to be sensitive to individual hydration layers when operated with cantilever oscillation amplitudes between 0.8 and

3.2 nm. The authors established that structured water layers were present in the case of lipid bilayers in the gel phase but not in the fluid phase and thus hydration effects should be considered as an integral component in cell membrane theory.

16.2.2 Technical Progresses

FM-AFM was originally introduced by Albrecht et al. in 1991 to operate dynamic-mode AFM in ultrahigh vacuum (UHV) environment [2]. Since the first demonstration of true atomic resolution in 1995 [22, 23], FM-AFM has been used for imaging various surfaces at subnanometer resolution. Until recently, however, the subnanometer-resolution imaging capability of FM-AFM had been limited to UHV environments.

In 2005, Fukuma et al. presented a way to overcome this limitation. True molecular-resolution imaging of a polydiacetylene single crystal was demonstrated in vacuum, air and liquid with a specially developed multi-environment FM-AFM [24]. True atomic-resolution imaging in liquid by FM-AFM was also demonstrated by imaging mica in water [25]. This technical innovation was brought about by major improvements in instrumentation and operating conditions, namely; deflection sensor, oscillation amplitude, and stiffness of the cantilever.

First of all, a stiff cantilever is necessary to reduce the cantilever thermal vibration as well as to avoid instabilities known as "jump-to-contact." True atomic- or molecular-resolution imaging requires a vertical resolution better than 10 pm. The root-mean-square (RMS) amplitude of the cantilever thermal vibration $\langle z_{\mathrm{th}} \rangle$ is given by

$$\langle z_{\mathrm{th}} \rangle = \sqrt{\frac{k_{\mathrm{B}} T}{k}}, \tag{16.3}$$

where k_{B}, T and k shows Boltzmann's constant, absolute temperature and the cantilever spring constant, respectively. This equation shows that thermal vibration of less than 10 pm requires a cantilever stiffness higher than 40 N/m. Fukuma et al. employed a cantilever with a nominal spring constant of 42 N/m instead of soft cantilevers (<1 N/m) typically used for in-liquid applications [26]. Note that it is possible to reduce the thermal vibration amplitude via the gentle contact of the tip with the surface, such as in contact-mode AFM. However, this method can often prohibit the precise control of the vertical tip position at the atomic-scale transient regime between "contact" and "non-contact", a capability essential for "true" atomic- and molecular-resolution imaging as well as for atomic-scale manipulation.

Secondly, small amplitude oscillation is essential to enhance the sensitivity to the short-range interaction forces and thereby obtaining high spatial resolution. The RMS amplitude of the noise in z (δz) caused by the frequency noise (δf) is given by [27],

$$\delta z = \frac{\delta f}{\partial \Delta f / \partial z}. \tag{16.4}$$

Giessibl et al. described that frequency noise is proportional to A^{-1} whereas $\partial \Delta f / \partial z$ is constant for small amplitudes and proportional to $A^{-3/2}$ for large amplitudes, hence the existence of an optimal amplitude [28]. This calculation showed that the optimal amplitude is of the order of the decay length of the force components. As for the short-range interaction force, this typically corresponds to the values less than 0.5 nm. Fukuma et al. used an oscillation amplitude of 0.2–0.3 nm [26] while the amplitude typically used for in-liquid application is larger than 2–3 nm.

Finally, the use of a low noise cantilever deflection sensor is necessary for the stable oscillation of a stiff cantilever with small amplitude as well as for ensuring thermal-noise-limited performance [24]. In FM-AFM, the deflection signal is used for generating the excitation signal as well as for detecting the frequency shift. Thus, stable self-oscillation with a small amplitude requires a low noise deflection signal. In addition, stiffer cantilevers make it more difficult to achieve thermal-noise-limited performance in FM-AFM [29]. The peak value of the power spectrum density (PSD) of the cantilever thermal vibration $(z_{\mathrm{th}})_{\mathrm{peak}}$ is given by,

$$(z_{\mathrm{th}})_{\mathrm{peak}} = \sqrt{\frac{2k_{\mathrm{B}}TQ}{\pi f_0 k}}, \tag{16.5}$$

where f_0 and Q are resonance frequency and the Q factor of the cantilever. Assume that $k = 40\,\mathrm{N/m}$, $Q = 10$, $f_0 = 130\,\mathrm{kHz}$, $(z_{\mathrm{th}})_{\mathrm{peak}}$ is 71 $\mathrm{fm}/\sqrt{\mathrm{Hz}}$. To reduce the influence of the deflection sensor to less than 10% of this value, the deflection noise from the sensor should be less than $71 \times 1/3 = 24\ \mathrm{fm}/\sqrt{\mathrm{Hz}}$. Whilst the deflection PSD from the sensor is 100–1,000 $\mathrm{fm}/\sqrt{\mathrm{Hz}}$, the PSD of the deflection sensor developed by Fukuma et al. in 2005, was 17 $\mathrm{fm}/\sqrt{\mathrm{Hz}}$ [24]. Details of the instrumentation required to achieve this noise performance are described in the previous chapter.

The impact of the technical innovation on the field of AFM research stimulated subsequent instrumentation development and additional exploration of these technologies for use in biological applications. Fukuma et al. further reduced the deflection noise density of the optical beam deflection sensor to 5.7 fm/Hz [29] and utilized these techniques in the investigations of biological materials [30–32] They also showed that true atomic resolution can be obtained not only by FM-AFM but also by phase-modulation AFM (PM-AFM) [33] when operated with a low noise deflection sensor, a stiff cantilever and small amplitude. Hoogenboom et al. obtained atomic-scale images of mica in liquid with a low-noise Fabry-Perot interferometer [19]. These technical advancements opened up the possibility of subnanometer-scale investigations on biological systems directly under physiological environment.

16.2.3 Biological Applications

In 1993, Ohnesorge et al. presented the first atomic-resolution image obtained in liquid by contact-mode AFM [34]. Compared to contact-mode AFM, FM-AFM has three major advantages: (1) precise control of the vertical tip position, (2) high spatial resolution, and (3) capability of imaging isolated molecules. Here, we show FM-AFM applications for biological systems, highlighting these three advantages.

Hydration Layers

In contact-mode AFM, a soft ($<1\,\mathrm{N/m}$) cantilever is generally used to obtain sufficient force sensitivity. However, the short-range attractive force at the atomic-scale non-contact regime, often presents a large force gradient exceeding the cantilever spring constant thus causing a cantilever instability known as "jump-to-contact". In addition, soft cantilevers can suffer from large thermal fluctuations, which can reduce control of the vertical tip position. In FM-AFM, the high stiffness of the cantilever, together with the restoring force of the vibrating cantilever, helps to avoid such instabilities, giving precise control over the tip vertical position at the atomic-scale contact/noncontact regime. Here, we present a biological application making the best use of this advantage [30].

Water molecules adjacent to biological membranes can potentially play a key role in the biological processes, particularly when they form hydration layers in which the water molecules are partially ordered due to interactions with the membrane, through dipole potentials or hydrogen bonding. If such hydration layers exist, they should alter the local interaction potential at the water/lipid interface, which can significantly influence the function of membrane proteins and molecular transport across the membranes. FM-AFM has a unique capability of measuring local interaction potentials with a nanometer-scale cross-section, using a sharp tip as a force probe. This capability is ideal to directly probe the interaction forces that nanoscale objects (e.g., proteins and solvated ions) would experience when they approach a membrane surface.

Figure 16.3 shows an example of such applications: a Δf vs. distance curve measured on a mica supported dipalmitoylphosphatidylcholine (DPPC) bilayer in phosphate buffer saline (PBS) solution. The Δf vs. distance curves obtained on the DPPC bilayer typically show an oscillatory force profile with one or two peaks. The averaged separation of the two peaks is $0.28 \pm 0.05\,\mathrm{nm}$. This distance is in agreement with the size of a water molecule and hence suggests that the oscillatory force profile corresponds to the sequential removal of ordered water molecules.

Tip–sample distance feedback regulation in liquid-environment FM-AFM operates based on the assumption that Δf increases with decreasing tip–sample separation, such as in the force branches indicated by arrows (1)–(3) in Fig. 16.3b. Therefore, if the Δf vs. distance curve shows an oscillatory profile,

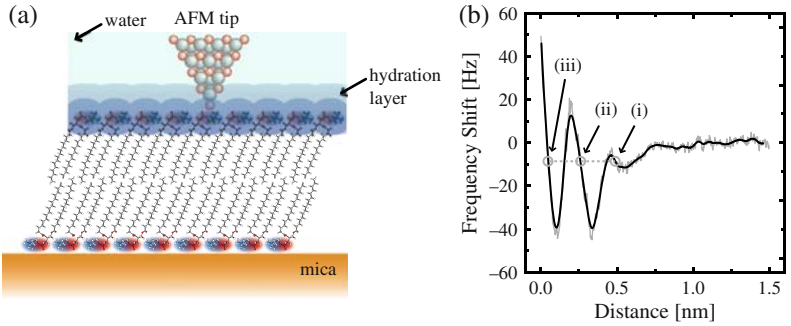

Fig. 16.3. (**a**) A DPPC bilayer formed on mica investigated by AFM in liquid. (**b**) Δf vs. distance curve measured on the DPPC bilayer in the PBS solution, showing oscillatory profile with two peaks. The smoothed line (*solid*) is obtained by averaging the raw data (*shaded*) over the distance range of 0.02 nm from each data point. (Reused with permission from Fukuma et al. [30] Copyright 2007, Biophysical Society)

the feedback can operate at multiple tip positions corresponding to one setpoint as indicated by the circles in Fig. 16.3b. Thus, the tip can spontaneously jump between those positions even if the setpoint is left unchanged.

Figure 16.4 shows an example of such spontaneous jumps during FM-AFM imaging of the DPPC bilayer in PBS solution. In the image shown in Fig. 16.4a, the tip is scanned from the lowest terrace (Terrace 1) and as the imaging progresses the tip jumps spontaneously twice. Terrace 1 shows a highly ordered arrangement of bright spots separated by 0.50 ± 0.05 nm along the stripes. The first jump of 0.26 nm (Terrace 1–2) results in subtle changes to the image although discrete corrugations are still observed. The second jump of 0.23 nm (Terrace 2–3) results in a less-ordered contrast although imaging resolution is still high. The heights of the spontaneous jumps (0.29 ± 0.06 nm) agree well with the size of a water molecule and the peak distance of the oscillatory force profile (0.28 ± 0.05 nm). This confirms that the tip is jumping between water layers and the individual layers are imaged with molecular-scale corrugations of the lipid headgroups. The result shows that the small loading force during FM-AFM imaging makes it possible to visualize weak interaction potentials presented by the water molecules adjacent to the biological membrane.

Lipid-Ion Network

In contact-mode AFM, long-range and short-range interaction forces are detected with equal sensitivity. In FM-AFM, the reduction of cantilever oscillation amplitude enhances the sensitivity to the short-range interaction force, and, at the same time, reduces the sensitivity to the long-range interaction force, thus giving higher spatial resolution than contact-mode AFM [28, 35].

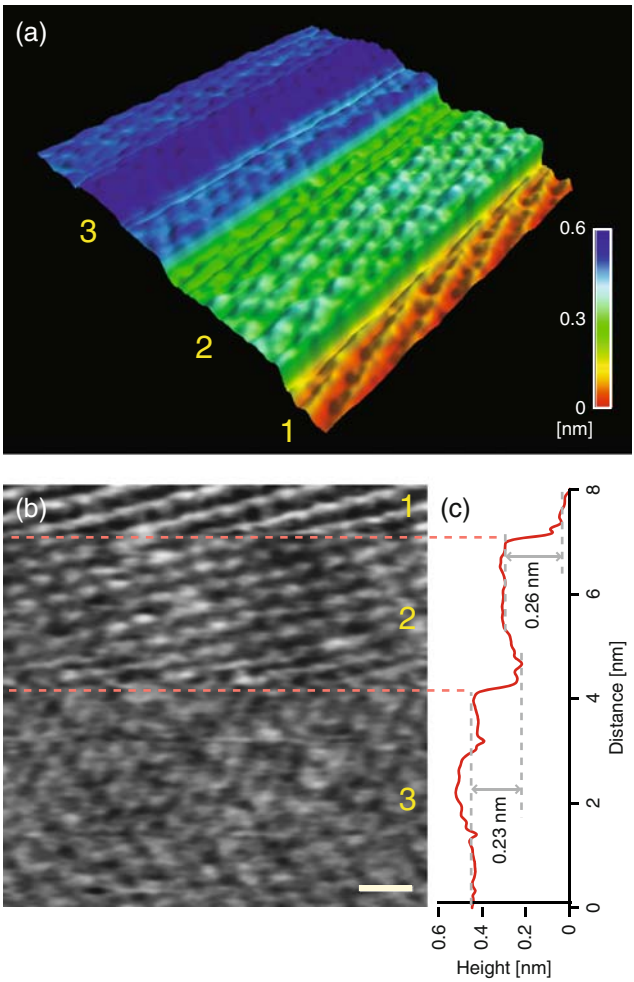

Fig. 16.4. (**a**) FM-AFM image of the DPPC bilayer in phosphate buffer solution showing spontaneous jumps during imaging. $8 \times 8\,\mathrm{nm}^2$, Tip velocity: 120 nm/s. Imaging speed: 85 s/frame. (**b**) Line-by-line flattened image of (**a**). Scale bar: 1 nm, Height range: 0.1 nm (*black to white*). Fast and slow scan directions: *left to right* and *top to bottom*. The regions indicated by the numbers 1, 2, and 3 correspond to the Terraces 1, 2, and 3 in (**a**). (**c**) Line-averaged height profile of (**b**) plotted along the slow scan direction. (Reused with permission from Fukuma et al. [30] Copyright 2007, Biophysical Society)

The following example of the use of FM-AFM in a biological application highlights this advantage, showing the unprecedented spatial resolution of 90 pm in liquid [31].

Under physiological conditions, biological membranes are surrounded by an electrolytic solution containing various metal cations. The influence of

these cations on membrane structure and stability has been studied intensively using model lipid bilayers. The addition of salts can trigger lipid bilayer phase separation [36–38], and vesicle aggregation and fusion processes [39,40]. The striking influence of the ions on membrane structure has highlighted the importance of lipid-ion interactions in biological processes. So far, a number of spectroscopy experiments have revealed that metal cations specifically interact with negatively charged moieties of the lipid headgroups [41–44]. These experiments, together with theoretical simulations [45], support the theory that individual ions may be interacting with multiple headgroups to form complex "lipid-ion networks" (Fig. 16.5a). This concept has been used to explain the observed influence of such ions in the enhanced mechanical strength of membranes [46] and the reduced mobility of the lipid molecules therein [47]. However, it has been a great challenge to experimentally access such lipid-ion networks due to the lack of a viable method for investigation of local lipid-ion interactions with Angstrom resolution. FM-AFM is an ideal tool for this, allowing direct investigation of the local lipid-ion networks formed at water/lipid interface.

Sequential FM-AFM images taken on the DPPC bilayer in PBS solution (Fig. 16.5) reveal that some of the surface groups change their configurations upon formation or disappearance of lipid-ion networks. For example, Subunit 1 is not pairing with another subunit in Fig. 16.5b while a pair of Subunits 3 and 4 appears in the next image (Fig. 16.5c) but with a darker contrast than other subunits, suggesting the lower height of this headgroup. It is likely that this particular headgroup was temporarily at an irregular tilt angle due to the interaction between Subunit 1 and 2 against the slight height difference when the first image was taken.

The observed structural changes due to the formation and disappearance of the lipid-ion networks indicates that the negatively charged phosphate groups are sharing the positive charge of cations, by which an attractive electrostatic force is exerted on all the headgroups involved in the network. The attractive

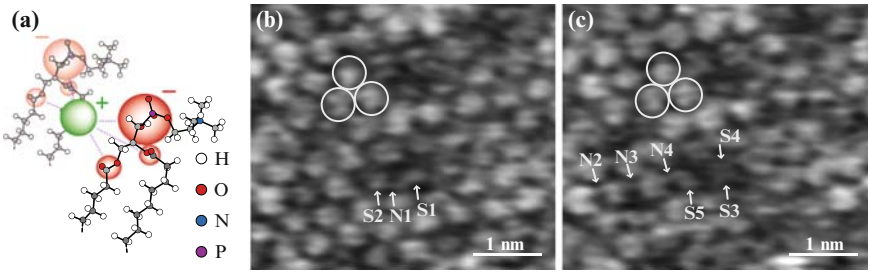

Fig. 16.5. (**a**) The lipid-ion complex formed the lipid/water interface. (**b**) and (**c**) Sequential FM-AFM images of the same area of the DPPC bilayer in PBS solution. Height range: 0.1 nm. Tip velocity: 120 nm/s. Imaging speed: 85 s/image (Reused with permission from Fukuma et al. [31] Copyright 2007, American Physical Society)

interaction force mediated through such complex lipid-ion networks should bind the headgroups together and increase the global mechanical strength of the membrane. In fact, it has been shown that the addition of metal cations increases the mechanical strength of the DPPC bilayer [46]. The FM-AFM images presented here reveal the submolecular-scale origin of such an influence of ions on the mechanical properties of the biological membrane.

Amyloid Fibrils

In contact-mode AFM, scanning the tip in contact with the surface inevitably causes a large friction force. This has hindered nondestructive imaging of isolated molecules or assemblies weakly bound to the substrate. As the vertical motion of the cantilever in dynamic-mode AFM dramatically reduces the lateral friction force, FM-AFM should be capable of imaging molecular-scale surface structures of such isolated systems. This capability has been demonstrated by imaging amyloid fibrils in PBS solution as described in the following section [32].

Amyloid fibrils are formed from a variety of proteins which are normally soluble in physiological solution [48, 49]. Under certain conditions, the precursor proteins misfold to form amyloid fibrils which are typically 10–30 nm in diameter and up to several micrometers in length as shown in Fig. 16.6a. The fibrils are insoluble β-sheet structures that can form aggregates in tissues and organs known as amyloid deposits. These deposits are found in a range of

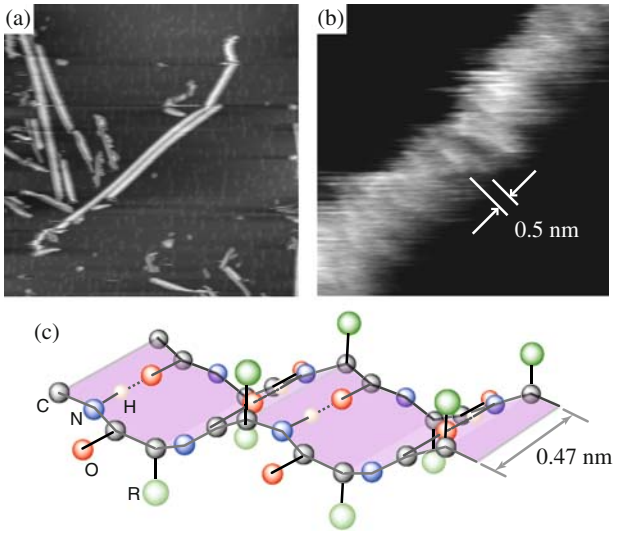

Fig. 16.6. FM-AFM images of IAPP fibrils on mica in PBS solution (**a**) 800 × 800 nm, $\Delta f = -55$ Hz, tip velocity: 1 μm/s. (**b**) 10 × 10 nm, $\Delta f = +50$ Hz, tip velocity: 195 nm/s. (**c**) Schematic model of the β-strands. (Reused with permission from Fukuma et al. [32] Copyright 2008, Institute of Physics)

neurodegenerative diseases such as Alzheimer's, Parkinson's and Huntington's disease [48]. Understanding the structure of amyloid fibrils is essential for elucidating the nucleation and kinetics of fibrillation in relation to the pathogenic pathway of amyloidoses.

Figure 16.6a, b show FM-AFM images of amyloid fibrils formed from the islet amyloid polypeptide (IAPP) deposited on mica in PBS solution. IAPP fibrils are associated with type 2 diabetes when deposited in pancreatic islets [50], The image shows finely striped features perpendicular to the fibril axis. The distance between adjacent stripes is approximately 0.5 nm. A previous X-ray diffraction study suggested the existence of periodic structure along IAPP fibril axes with a characteristic spacing of 0.47 nm [51]. Since this periodicity corresponds to hydrogen bond spacing between the β-strands (Fig. 16.6c), the periodic structure was attributed to the alignment of the β-strands perpendicular to the fibril axis [51]. The fine stripes observed in the FM-AFM image have comparable spacing aligned perpendicular to the fibril axis. Therefore, the striped features are attributed to the β-strands of IAPP fibrils. This demonstrates the possibility of FM-AFM to visualize individual β-strands in real space in a physiologically-relevant liquid environment.

16.3 Future Prospects

The theory and instrumentation of liquid-environment FM-AFM has dramatically progressed in the last 10 years. This has enabled quantitative measurements of conservative and dissipative forces and subnanometer-resolution imaging with piconewton-order loading forces at the solid/liquid interface. The biological applications presented here demonstrate that FM-AFM is capable of probing and visualizing the local interactions between the bio-molecules and surrounding physiological environment (i.e., water molecules and ions) as well as the structures of bio-molecules themselves.

There are still a number of technical issues and challenges to be overcome in order to make the technique more useful in practical studies. Among the most urgent of these are improvements in operation speed. This is important not only for visualizing dynamic processes but also for high-resolution imaging of large areas containing inhomogeneous complexes and also non-destructive high-resolution imaging of large isolated bio-molecules. These applications may not require high frame rate but do require a high feedback bandwidth. As up to now, imaging speed was not a major priority for applications performed in vacuum, there is considerable room for improvement.

Another important issue is the stability. As seen in Fig. 16.4, multiple feedback points can exist at the solid/liquid interface. Although this could be a useful tool for visualization of individual hydration layers, it can also make it difficult to control vertical tip position. This is not a simple technical issue as the solid/liquid interface inherently has a three-dimensional extension. This issue may be solved by employing the three-dimensional imaging technique developed for applications in UHV at low temperature [52], together with the

feedforward drift compensation technique developed for atom manipulation at room temperature [53].

There are also many application areas that have not been explored fully, including biology and electrochemistry. So far, the latter has not been explored at all by FM-AFM. This is partly because of the existence of electrochemical STM. However, there are emerging interests in the electrochemical processes of organic and biological molecules in relation to their applications to organic- and bio-electronics. Since these non-conductive molecules cannot be imaged by STM, we expect that the application of FM-AFM to this area will also grow in the near future.

References

1. F.J. Giessibl, Phys. Rev. B **56**, 16010 (1997)
2. T.R. Albrecht, P. Grütter, D. Horne, D. Ruger, J. Appl. Phys. **69**, 668 (1991)
3. U. Dürig, Appl. Phys. Lett. **75**, 433 (1999)
4. J.. Sader, S.P. Jarvis, Appl. Phys. Lett. **84**, 1801 (2004)
5. T. Uchihashi et al., Appl. Phys. Lett. **85**, 3575 (2004)
6. J.E. Sader, S.P. Jarvis, Phys. Rev. B **74**, 195424 (2006)
7. G.B. Kaggwa, J.I. Kilpatrick, J.E. Sader, S.P. Jarvis, Appl. Phys. Lett. **93**, 011909 (2008)
8. S.P. Jarvis, A. Oral, T.P. Weihs, J.B. Pethica, Rev. Sci. Instrum. **64**, 3515 (1993)
9. A. Buguin, O.D. Roure, P. Silberzan, Appl. Phys. Lett. **78**, 2982 (2001)
10. M.J. Higgins, C.K. Riener, T. Uchihashi, J.E. Sader, Nanotechnology **16**, S85 (2005)
11. A.D.L. Humphris, J. Tamayo, M.J. Miles, Langmuir **16**, 7891 (2000)
12. A.D.L. Humphris, M. Antognozzi, T.J. McMaster, M.J. Miles, Langmuir **18**, 1729 (2002)
13. M. Higgins, J.E. Sader, S.P. Jarvis, Biophys. J. **90**, 640 (2006)
14. J. Tamayo, A.D.L. Humphris, R.J. Owen, M.J. Miles, Biophys. J. **81**, 526 (2001)
15. S.P. Jarvis et al., J. Phys. Chem. B **104**, 6091 (2000)
16. H. Sekiguchi et al., Appl. Surf. Sci. **210**, 61 (2003)
17. C.-W. Yang et al., Nanotechnology **18**, 084009 (2007)
18. D. Ebling, H. Hölscher, B. Anczykowski, Appl. Phys. Lett. **89**, 203511 (2006)
19. B.W. Hoogenboom et al., Appl. Phys. Lett. **88**, 193109 (2006)
20. B.W. Hoogenboom, K. Suda, A. Engel, D. Fotiadis, **370**, 246 (2007)
21. M. Higgins et al., Biophys. J. **91**, 2532 (2006)
22. F.J. Giessibl, Science **267**, 68 (1995)
23. S. Kitamura M. Iwatsuki, Jpn. J. Appl. Phys. Part II **34**, L145 (1995)
24. T. Fukuma et al., Rev. Sci. Instrum. **76**, 053704 (2005)
25. T. Fukuma, K. Kobayashi, K. Matsushige, H. Yamada, Appl. Phys. Lett. **87**, 034101 (2005)
26. T. Fukuma et al., Appl. Phys. Lett. **86**, 034103 (2005)
27. edited by S. Morita, R. Wiesendanger, E. Meyer (Eds.), *Noncontact Atomic Force Microscopy (Nanoscience and Technology)* (Springer, Berlin, 2002)
28. F.J. Giessibl, H. Bielefeldt, S. Hembacher, J. Mannhart, Appl. Surf. Sci. **140**, 352 (1999)

29. T. Fukuma, S.P. Jarvis, Rev. Sci. Instrum. **77**, 043701 (2006)
30. T. Fukuma, M.J. Higgins, S.P. Jarvis, Biophys. J. **92**, 3603 (2007)
31. T. Fukuma, M.J. Higgins, S.P. Jarvis, Phys. Rev. Lett. **98**, 106101 (2007)
32. T. Fukuma, A.S. Mostaert, S.P. Jarvis, Nanotechnology **19**, 384010 (2008)
33. T. Fukuma, J.I. Kilpatrick, S.P. Jarvis, Rev. Sci. Instrum. **77**, 123703 (2006)
34. F. Ohnesorge, G. Binnig, Science **260**, 1451 (1993)
35. F.J. Giessibl, S. Hembacher, H. Bielefeldt, J. Mannhart, Science **289**, 422 (2000)
36. M. Rappolt, G. Pabst, H. Amenitsch, P. Laggner, Coll. Surf. A **183–185**, 171 (2001)
37. M. Ross, C. Steinen, H.-J. Galla, A. Janshoff, Langmuir **17**, 2437 (2001)
38. J.T. Groves, S.G. Boxer, H.M. McConnell, J. Phys. Chem. B **104**, 11409 (2000)
39. S. Ohki, N. Düzgüneş, K. Leonards, Biochemistry **21**, 2127 (1982)
40. S. Ohki, K. Arnold, Coll. Surf. B **18**, 83 (2000)
41. L. Herbette, C.A. Napolitano, R.V. McDaniel, Biophys. J. **46**, 677 (1984)
42. C. Altenbach, J. Seelig, Biochemistry **23**, 3913 (1984)
43. T.R. Hermann, A.R. Jayaweera, A.E. Shamoo, Biochemistry **25**, 5834 (1986)
44. H. Binder, O. Zschörnig, Chem. Phys. Lipids **115**, 39 (2002)
45. M.L. Berkowitz, D.L. Bostick, S. Pandit, Chem. Rev. **106**, 1527 (2006)
46. S. Garcia-Manyes, G. Oncins, F. Sanz, Biophys. J. **89**, 1812 (2005)
47. R.A. Böckmann, A. Hac, T. Heimburg, H. Grubmüller, Biophys. J. **85**, 1647 (2003)
48. P. Westermark et al., Amyloid **12**, 1 (2005)
49. P. Westermark, FEBS J. **272**, 5942 (2005)
50. P. Westermark, C. Wernstedt, E. Wilander, D.W. Hayden, Proc. Natl. Acad. Sci. USA **84**, 3881 (1987)
51. O.S. Makin, L.C. Serpell, J. Mol. Biol. **335**, 1279 (2004)
52. H. Hölscher, S.M. Langkat, A. Schwarz, R. Wiesendanger, Appl. Phys. Lett. **81**, 4428 (2002)
53. M. Abe et al., Appl. Phys. Lett. **90**, 203103 (2007)